Solar Energy 242 (2022) 256–266

Contents lists available at ScienceDirect

Solar Energy

journal homepage: www.elsevier.com/locate/solener

Accelerating the reaction kinetics of K_2CO_3 through the addition of CsF in the view of thermochemical heat storage

Natalia Mazur [a,b], Henk Huinink [a,b,*], Hartmut Fischer [c], Pim Donkers [d], Olaf Adan [a,b,c,d]

[a] Department of Applied Physics, Eindhoven University of Technology, Den Dolech 2, 5600 MB Eindhoven, the Netherlands
[b] Eindhoven Institute for Renewable Energy Systems, Eindhoven University of Technology, PO Box 513, 5600 MB Eindhoven, the Netherlands
[c] TNO Materials Solutions, High Tech Campus 25, 5656 AE Eindhoven, the Netherlands
[d] Cellcius, Horsten 1, 5612 AX Eindhoven, the Netherlands

ARTICLE INFO

Keywords:
Thermochemical energy storage
Salt hydrates
Reaction kinetics
Thermal analysis

ABSTRACT

Potassium carbonate (K_2CO_3) is a promising thermochemical heat storage material (TCM). However, it suffers from hysteresis between (de)hydration temperatures and poor reaction kinetics close to equilibrium conditions. Both aspects are caused by a nucleation barrier and low ionic mobility close to equilibrium. This study investigates the impact of caesium fluoride (CsF) incorporated through recrystallisation on the phase transitions. The composition studies show that K_2CO_3 and CsF react during synthesis, forming KF, which points to the formation of Cs_2CO_3. The secondary phases are not incorporated into the crystal structure but reside between the main phase's grain cracks due to capillary forces. Because the secondary phases are highly hygroscopic, they promote surface mobility by forming a liquid-like layer even at low water vapour pressures. As the effect of their presence, hydration kinetics are enhanced significantly in all investigated conditions, with the most pronounced impact when hydration of K_2CO_3 is inherently inhibited. The benefits manifest themselves through a faster reaction rate and shorter induction period. The dehydration is enhanced by the presence of the additive mainly far away from equilibrium conditions. Close to the equilibrium, the dehydration of the composite proceeds in an unusual 2-step manner, where the second step is much slower than the dehydration of pure K_2CO_3. The enhancement of dehydration kinetics is ascribed to the formation of defects during recrystallisation. The lowering of dehydration rates close to equilibrium is attributed to diffusion issues due to excess of a deliquescent phase present in the system.

1. Introduction

Thermochemical heat storage in salt hydrates is an emerging domestic energy storage technology. The system is designed around a reversible reaction between water vapour and a salt hydrate. The salt reacts exothermally with water vapour forming a salt hydrate during discharge while the generated heat is harvested for domestic purposes. During charge, the salt hydrate is dehydrated with the aid of heat, which is thus stored in the material for later use. Over the years, many different salt hydrates have been investigated for this purpose (Afflerbach and Trettin, 2019; Clark et al., 2022; Donkers et al., 2017; N'Tsoukpoe et al., 2014; Richter et al., 2018). Those studies have shown that many materials suffer from similar limitations, such as reaction hysteresis, poor power output and cyclic instability. One of the investigated candidates is potassium carbonate, K_2CO_3. It emerged as a thermochemical material (TCM) due to its desirable phase transition conditions and its suitable character for domestic use (non-toxic, cheap and chemically stable) (Donkers et al., 2017; Zhao et al., 2022). A closer study of the material has revealed that it is cyclically stable, but there is a large discrepancy between (de)hydration temperatures and the calculated equilibrium temperature (Sögütoglu et al., 2018).

A subsequent study by Sögütoglu et al. (Sögütoglu et al. 2021, 2019) has shown limiting kinetics in near-equilibrium conditions, named the metastable zone (MSZ). This study proposed that hydration proceeds through a formation of a wetting layer on top of the anhydrate, its local dissolution and subsequent crystallisation of the hydrated phase. Furthermore, it is postulated that supersaturation above the equilibrium conditions governs mobility within the wetting layer and determines reaction speed.

Similar limiting kinetics have been found in $MgSO_4$ 7–6 H_2O

* Corresponding author.
E-mail address: h.p.huinink@tue.nl (H. Huinink).

https://doi.org/10.1016/j.solener.2022.07.023
Received 11 March 2022; Received in revised form 29 June 2022; Accepted 14 July 2022
Available online 21 July 2022

transition (Linnow et al., 2014). To mitigate this issue, $MgSO_4$ has been recrystallised with other salts. Adding $ZnSO_4$ (Ur Rehman et al., 2019) or $MgCl_2$ (Posern and Kaps, 2010) resulted in a higher heat of sorption than pure $MgSO_4$. In the case of $MgSO_4$-$MgCl_2$ mixtures, it was attributed to the additional phase transition in the form of deliquescence of $MgCl_2$ at the measurement conditions. In another study, the addition of $SrCl_2$ (Li et al., 2020) increased both hydration kinetics and heat of sorption and has proven to be cyclically stable. In all cases, improvements have been observed for an optimum salt ratio.

In contrast, some of the investigated salt mixtures have shown undesirable side effects, such as local deliquescence or lowering of energy density. The work conducted on $MgSO_4$ salt mixtures shows that recrystallising a salt hydrate that suffers from metastable behaviour with another salt might result in an overall better TCM composite material. It also illustrates that the relationship between deliquescence points of salts in the mixture and the conditions at which measurements are conducted is of utmost importance. Finally, deliquescence of the minor phase seems to enhance reaction kinetics, but it also limits the operating window by lowering the maximum humidity the TCM composite can be exposed to before the entire mixture undergoes mutual deliquescence. Work conducted on other salt hydrate mixtures further supports those findings (Li et al., 2020; Rammelberg et al., 2016; Rammelberg et al., 2013).

In this paper, we investigate the impact of caesium fluoride, CsF, on the reaction kinetics of K_2CO_3. CsF is a highly hygroscopic salt with a deliquescence point at 3.39 % RH (≈ 1 mbar) at 25 °C (Greenspan, 1976) and the ability to form hydrates (Aylward and Findlay, 2008). Based on its extremely low deliquescence point, it was chosen as a proof of concept for synthesising TCM composites based on K_2CO_3. The aim is to enhance the formation of a wetting layer on the surface of K_2CO_3 through the deliquescence of CsF. Through that, we want to investigate the influence of the modified wetting layer on the reaction kinetics and MSZ width. Furthermore, we will examine the impact of the additive in varying quantities on (de)hydration behaviour at a range of conditions to gain an overview of the benefits and drawbacks a deliquescent additive can have on the phase transitions of K_2CO_3.

2. Materials and methods

2.1. Composite synthesis

Salt mixtures were prepared from K_2CO_3 (LabKem, Spain) and CsF (Alfa Aesar, Germany). First, as-received powders were completely dehydrated in an oven at 130 °C. The anhydrous powders were then weighed out and dissolved in deionised water in an appropriate ratio to obtain 1 M K_2CO_3 and 0.1 M CsF solutions. The resulting solutions were then mixed in a beaker at the desired ratio, which after evaporation of water should yield desired molar ratio of anhydrous K_2CO_3 to anhydrous CsF, summarised in column 1 of Table 1. Excess water was first evaporated under constant stirring at 115 °C until a wet cake formed at the bottom of the beaker. The wet cake was then transferred to watch glass, and the remaining water was evaporated overnight in an oven at 130 °C. Finally, the obtained salt mixture was roughly ground with mortar and pestle and transferred into an airtight glass container for storage. According to the same procedure, pure K_2CO_3 was recrystallised from the 1 M solution as reference material.

The composition of the as-synthesised composites was checked with a Dionex ICS-90 ion chromatograph. Five samples of approximately 1 mg of the dry powder were taken, and each was dissolved in 10 mL of deionised water. The K^+ and Cs^+ ion concentrations were measured with ion chromatography and compared with known standards. The concentration of K^+ ions was compared against the Dionex cation standard solution, while the concentration of Cs^+ ions was compared against the standard solution prepared by dissolving a known amount of anhydrous Cs_2CO_3 (Alfa Aesar, Germany) in deionised water. Finally, the measured concentrations of K^+ and Cs^+ were compared to one another and are summarised in Table 1.

2.2. Characterisation

2.2.1. Powder X-ray diffraction

The impact of CsF on the crystal structure of K_2CO_3 was investigated with powder X-ray diffraction (PXRD). The analysis was conducted in Rigaku Miniflex 600 X-ray diffractometer (Cu Kα radiation; Be monochromator, $\lambda = 1.5419$ Å, 40 kV, 15 mA) equipped with a D/tex Ultra 1D detector and an Anton-Paar BTS500 heating stage. An in-house built humidifier was coupled to the heating stage and calibrated by determining the onset point of hydration of LiCl at 30, 40 and 50 °C (Sögütoglu et al., 2019). The desired water vapour pressure (p_{vap}) is obtained by mixing completely dry air with fully humidified air at a specific ratio and 800 mL/min flow rate. All measurements were done between 25 and 50 2θ with 0.02° step size and a 5°/min scan speed. Data analysis was conducted in Rigaku PDXL2 software coupled with Crystallography Open Database (COD) (Vaitkus et al., 2021).

The synthesised salt mixtures were investigated in their anhydrous and hydrated state, where the initial sample preparation was done ex-situ. Finely ground powders were dried overnight in an oven at 130 °C to obtain anhydrous salts. After loading the sample holder, it was placed in the heating stage and heated up to 130 °C under dry airflow for 30 min to remove any moisture absorbed during powder alignment in the sample holder. After 30 min, the stage was cooled down to 30 °C, and after 30 min of the equilibration period, the X-ray diffractogram was measured. To obtain hydrated salts, finely ground powders were placed in a desiccator with saturated $MgCl_2{\cdot}6H_2O$ solution (33 % RH (Greenspan, 1977) , approximately 8 mbar at 21 °C) until complete conversion was measured by monitoring the weight change (approximately 3 days). Those powders were then loaded into a sample holder and placed in the heating stage. Measurements were conducted at room temperature with no humidity control.

2.2.2. Scanning electron microscopy

In order to determine the placement of the additive within the salt mixture, synthesised powders were studied with scanning electron microscopy (SEM). Before SEM imaging, powder samples were completely dehydrated in an oven at 130 °C. Then, the dry powders were applied to a stub with carbon tape and immediately placed in the device to prevent

Table 1
Summary of investigated salt mixtures and the composition of synthesised composites measured with ion chromatography.

Sample composition [mol K_2CO_3: mol CsF]	K_2CO_3 content [wt%]	CsF content [wt%]	Measured composition [mol K_2CO_3: 1 mol CsF]
10:1	90.10	9.90	7.2 ± 0.3
20:1	94.79	5.21	19.2 ± 2
50:1	97.85	2.15	45.9 ± 3
100:1	98.91	1.09	99.4 ± 4
K_2CO_3	100	0	N/A

any hydration. The imaging was done in with JEOL Fei Quanta 600. The measurements done in backscatter mode (BSE) used a high vacuum, 10 kV accelerating current, and 3.0 spot size.

2.2.3. Dynamic vapour sorption

Sorption and deliquescence properties were investigated employing the dynamic vapour sorption (DVS) thermogravimetric method with Q5000 SA thermobalance from TA Instruments. Powders were ground and sieved between 50 and 164 μm and dried in an oven at 130 °C. Approximately 1 mg of powder was loaded into a glass crucible. The measurements were conducted under a nitrogen atmosphere with a fixed flow rate of 200 mL/min.

Each measurement on a composite material started with a 1 h in-situ drying step at 80 °C and 0 % RH. Subsequently, the chamber's temperature was lowered to 25 °C, and the mass was equilibrated under dry conditions. Then relative humidity (RH) was stepwise increased in 3 stages: 1) Hydration onset between 0 and 12 % RH in steps of 2 % RH; 2) Hydration completion between 12 and 27 % RH in steps of 5 % and 3) Deliquescence onset from 27 to 45 % RH in steps of 1 % RH. Each RH step lasted for 5 h.

2.2.4. Thermogravimetric analysis

Thermogravimetric analysis was done in a TGA851e of Mettler-Toledo equipped with an in-house built humidifier. The temperature of the TGA was calibrated using In, Zn and benzophenone calibration standards with defined melting point temperatures, with an accuracy of 0.2 °C. The humidifier was calibrated by looking for the deliquescence onset point at 25 °C of LiCl·H_2O, $MgCl_2$·6H_2O, K_2CO_3·1.5H_2O and Mg$(NO_3)_2$·6H_2O (Greenspan, 1977), resulting in an accuracy of 0.16 mbar.

Before the thermogravimetric (TGA) measurement, samples were ground in pestle and mortar and sieved between 50 and 164 μm particle fraction to ensure sample homogeneity. Approximately 5 mg of powder in a 40 μL aluminium pan by Mettler-Toledo was used in all TGA measurements. All experiments were conducted under a nitrogen atmosphere with a fixed flow rate of 300 mL/h.

The thermogravimetric measurements can be divided into three categories:

(1) Reaction onset points:
The impact of CsF on the reaction onset points which determine the MSZ width was investigated at a fixed vapour pressure of 12 mbar. The temperature was varied between 130 and 25 °C at a scanning rate of 1 °C/min. A 7 h long isobaric step at 25 °C was introduced between the temperature scans to ensure complete hydration before the following heating step. Onset points for the reaction were determined by looking for a rapid change in the 1st derivative of the mass-time curve plotted against measured sample temperature.

(2) Cyclic stability:
The reaction reversibility of composites was monitored over 10 (de) hydration cycles. First, dehydration was conducted at 130 °C and 0 mbar, where temperature and water vapour pressure were adjusted simultaneously. After dehydration, the temperature is lowered to 30 °C and equilibrated for 30 min in dry N_2 flow before water vapour is introduced to the system. Subsequent hydration was conducted at isobaric and isothermal conditions of 30 °C and 12 mbar.

(3) Reaction kinetics:
Before measuring reaction kinetics, samples were cycled 10 times according to the procedure described in the section above. It was done to exclude any effects related to pristine powders, which were observed in earlier studies (Sögütoglu et al., 2018; Stanish and Perlmutter, 1984a), where the phase transition behaviour of the first cycles deviated strongly from that of a material that has been (de) hydrated several times. Reaction kinetics were measured at isobaric and isothermal conditions listed in Fig. 1 and Table 2. Each measurement started with dehydration in-situ at 130 °C and 0 mbar. After that, the temperature was lowered and equilibrated in dry N_2 flow for 30 min. At this point, water vapour was introduced to the system, which marked t = 0 for hydration. The desired vapour pressure was held constant for several hours while the reaction progress was recorded. If hydration was investigated at very low p_{vap}, the vapour pressure was increased to 19 mbar to achieve full hydration in a short period of time before proceeding to dehydration measurement. Once the complete conversion was achieved, the vapour pressure was lowered to the desired value. This marked t = 0 for the dehydration reaction, which was monitored for several hours. The hydration and dehydration kinetics are evaluated at complementary supersaturation ratios defined as $p^*=p_{hyd}/p_{eq} = p_{eq}/p_{deh}$.

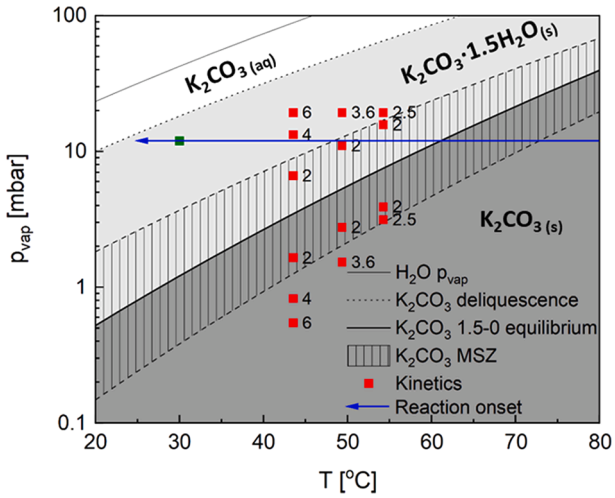

Fig. 1. Phase diagram of potassium carbonate adapted from (Sögütoglu et al., 2019). The dark grey zone indicates the region where K_2CO_3·1.5H_2O(s) is stable, and the light grey zone is where K_2CO_3(s) is stable. The hatched area indicates the metastable zone, where phase transitions are strongly inhibited. The blue arrow shows part of the 130–25 °C temperature scan at 12 mbar used to determine reaction onset points. The isobaric-isothermal kinetics measurements are indicated by red squares and hydration during cycling by a green square. Labels next to the red points specify p*. (For interpretation of the references to colour in this figure legend, the reader is referred to the web version of this article.)

Table 2
Summary of measurement conditions for reaction kinetics at paired supersaturation, p*, conditions.

Temperature [°C]	p hydration [mbar]	p dehydration [mbar]	p* [-]
30.0	12.0*		
43.5	19.0	0.6	6.0
43.5	13.3	0.8	4.0
43.5	6.7	1.7	3.0
49.0	19.7	1.5	3.6
49.0	11.1	2.8	2.0
54.0	19.7	3.9	2.5
54.0	15.8	3.2	2.0

* Isobaric-isothermal hydration conditions of cyclic stability investigation.

3. Results and discussion

3.1. Location of the additive in the composite

3.1.1. PXRD

We began our investigation of K_2CO_3-CsF composites by studying their crystal structure through PXRD. From the results summarised in Fig. 2, we see that the addition of CsF does not impact the lattice structure of K_2CO_3 (anhydrous or hydrated) since all primary reflections of the base salt are unchanged. The measured patterns are analogous to

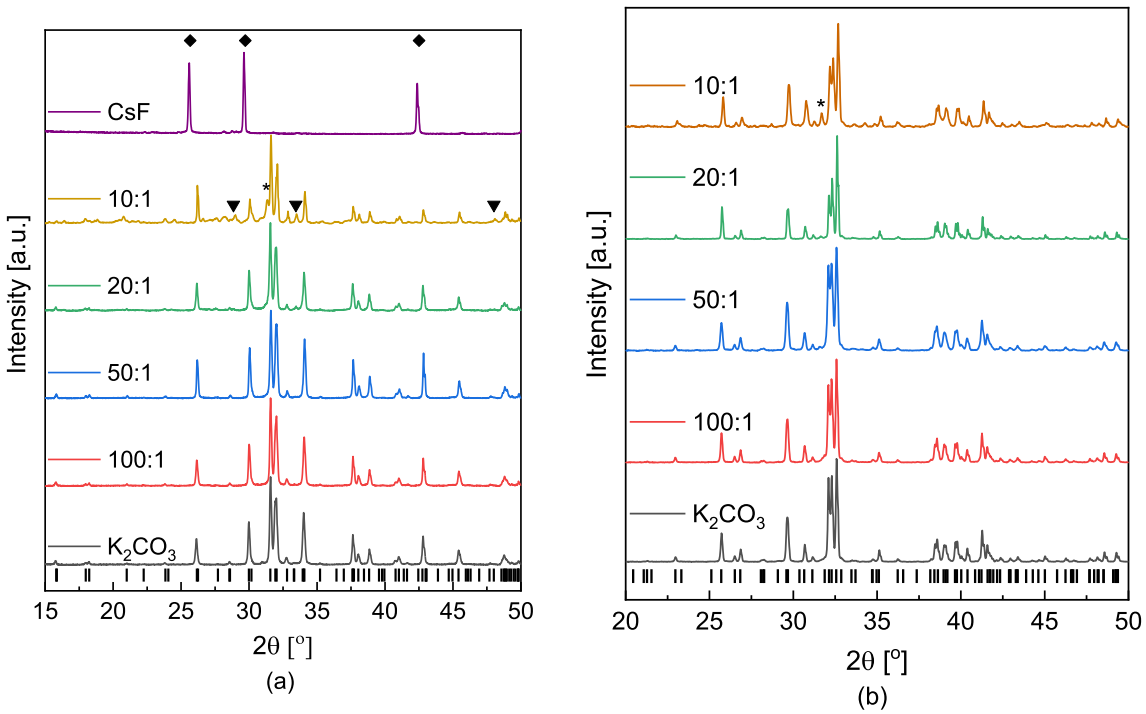

Fig. 2. Measured PXRD patterns of a) anhydrous samples compared with K_2CO_3 – COD 9,009,644 (Idemoto et al., 1998); ▼ KF-COD 9,008,652 (Wyckoff, 1963), ◆ CsF – COD 9,008,621 (Wyckoff, 1963) b) hydrated samples compared with $K_2CO_3{\cdot}1.5H_2O$ – COD 9,007,907 (Skakle et al., 2001). * marks an undefined peak.

the reference pattern, except for the 10:1 and 20:1 composites. In this case, we can see additional peaks belonging to KF (black triangles in Fig. 2a) and a single unidentified peak (marked with a star). The relative height of the (2,0,0) KF reflection (33.4 2θ) is 7.7 and 4 % for the 10:1 and 20:1 samples. Based on that, we can estimate the KF content in the respective samples to be 11.5 and 6 wt%. In the case of samples with lower CsF content, no secondary phases could be detected. This indicates that a reaction between K_2CO_3 and CsF occurred during preparation, and at least part of the additive was converted to KF. This process is highly plausible since the solubility of KF is lower than that of CsF (Aylward and Findlay, 2008). A simultaneous formation of Cs_2CO_3 is highly plausible, as the Cs-ions must pair with a counterion, and the only available cation is CO_3^{2-}. It would also explain why we did not identify any peaks belonging to CsF. Even if the reaction was only partial, with the detection limit of the device at 2 wt%, the content of any of the possible products of K_2CO_3-CsF recrystallisation is too low to be identified with high certainty. In the hydrated state, we have identified only $K_2CO_3{\cdot}1.5H_2O$. Since the measurements were conducted above the deliquescence point of any of the secondary phases (samples were hydrated at 33 % RH or approximately 8 mbar), as a salt solution, they were rendered invisible to the X-ray. Given that the measured XRD patterns correspond well with the reference patterns, we presume that the additive is not incorporated into the crystal structure but most likely is present as a secondary phase.

3.1.2. SEM – BSE

Considering we have not observed any significant changes in the crystal structure of either anhydrous or hydrated K_2CO_3, we have employed SEM-BSE to probe the location of the secondary phase within the salt mixture. Fig. 3 shows BSE images of composites and pure K_2CO_3 at 5000x magnification. We see significant contrast differences (highlighted by orange circles and arrows) in the composite when comparing the images. The number of the bright areas decreases with decreasing CsF content and turns into sporadic point inclusions. In the case of 50:1 and 100:1 samples, the contrast differences disappear. Pure K_2CO_3 presents a more uniform image with minor contrast fluctuations originating from the height differences within the sample and not from variations in the composition. Based on this, we presume that two separate phases are present in the composite sample and assume that the bulk of the sample, made up of the dark grey grains, is K_2CO_3. The bright areas between the grains and grain cracks are presumed to be Cs-rich because caesium is heavier than potassium, resulting in higher contrast. Those images further support the assumption that the additive is not incorporated into the K_2CO_3 crystal structure after recrystallisation, but instead, it decorates the grains on the surface. Most commonly, it resides between grains and grain cracks. Since the secondary phase is very deliquescent, the liquid phase will retract into small voids, such as cracks, during drying due to capillary action. This retraction of the liquid-like pockets and their small amounts in the 50:1 and 100:1 samples are most likely causes for the difficulties in their detection.

3.2. Water sorption by composites

In the next step, we look into the water sorption properties of composites. For this purpose, we have conducted DVS measurements at 25 °C between 0 and 45 % RH (0–14.3 mbar p_{vap}). Based on experimental conditions and the data from Fig. 1, we know that two major processes linked with mass increase can occur during the measurement. First, at lower vapour pressures, hydration takes place, and at a later stage, deliquescence occurs.

In Fig. 4, we see that hydration begins between 1 and 2 mbar, which is between previously published hydration onset at 2.6 mbar and equilibrium conditions of 0.80 mbar at 25 °C (Sögütoglu et al., 2019). In the case of composites, mass uptake begins at lower p_{vap} than in pure K_2CO_3, which is caused by the additive's hydration and/or deliquescence. Pure CsF undergoes deliquescence at approximately 1 mbar at 25 °C (Greenspan, 1976) and hydration at approximately 0.2 mbar (Aylward and Findlay, 2008; Glasser, 2014). Hydration of pure KF should take place at 4.7 mbar (Glasser, 2014) and deliquescence 9.8 mbar (Greenspan, 1976), which is well above the initial mass increase. Finally, the only thermodynamic data for Cs_2CO_3 is that for 0–3.5-hydrate transition, which should occur at 0.5 mbar (Glasser, 2014). Nevertheless, it is

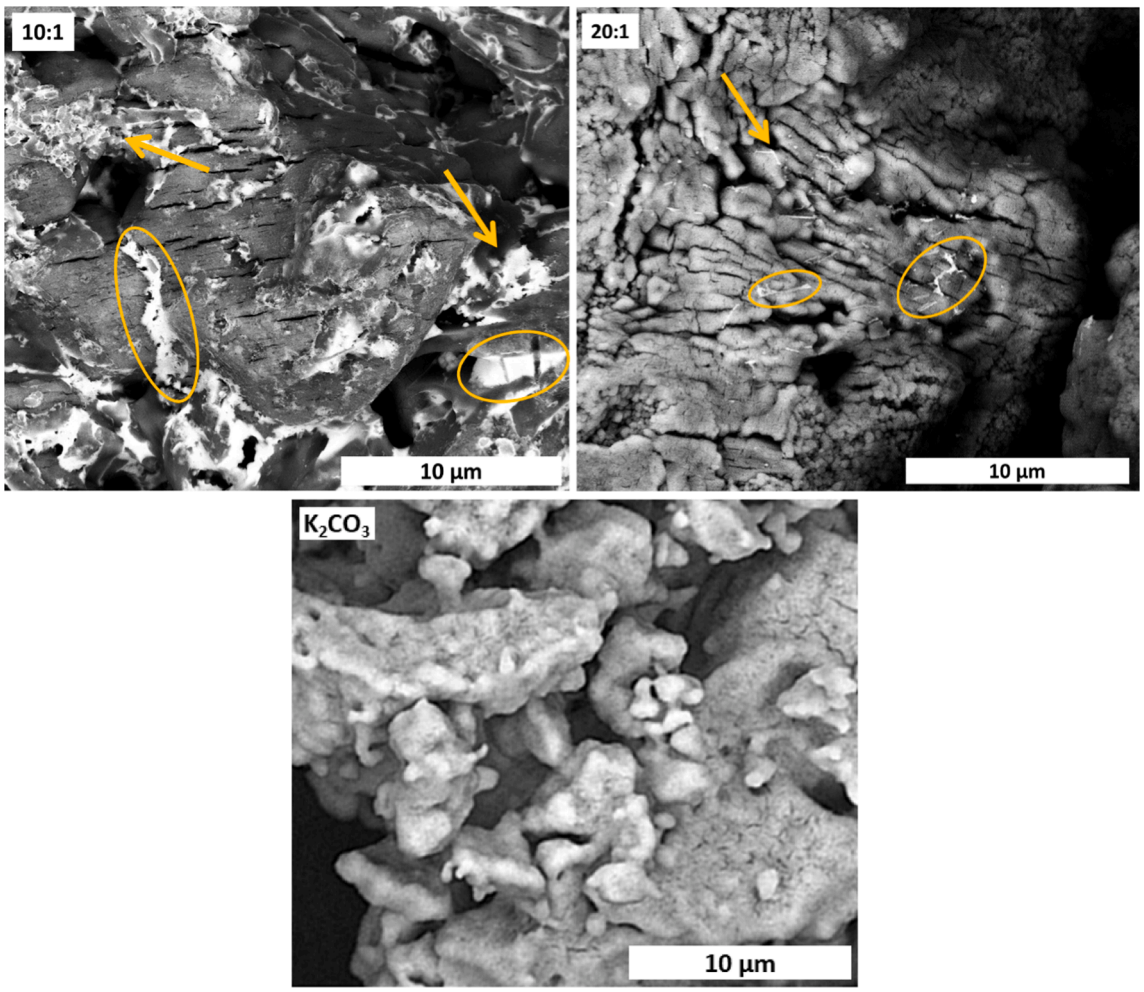

Fig. 3. Backscatter images of composites and pure K_2CO_3 and 5000x magnification. Orange circles and arrows highlight some of the secondary phase in the composites Images were taken at 10 kV and 3.0 spot size under high vacuum. (For interpretation of the references to colour in this figure legend, the reader is referred to the web version of this article.)

impossible to distinguish between those processes, especially in the presence of another salt, yet we can assign the water uptake at lower humidity to the presence of a secondary phase.

As the humidity increases, the water content in the sample increases. As a result, pure K_2CO_3 attains a plateau in the 5–12 mbar region, reaching total hydration with 0.193 g H_2O / g salt. On the other hand, the composites exhibit a continuous mass increase in the same region. Furthermore, the water content in that interval is larger than expected from the hydration of the individual constituents of the composite. Consequently, we assume that during hydration of K_2CO_3, at least partial deliquescence of the additive and thus liquid water accumulates in the sample. We thus suspect that a further dilution of the salt solution causes the slow mass increase in composites in the region where pure K_2CO_3 is stable (Li et al., 2020).

Finally, at $p_{vap} > 12$ mbar, we observe the second significant mass uptake, which corresponds to the deliquescence of K_2CO_3. We have defined the deliquescence onset points as the cross point between two tangents, as exemplified in the insert in Fig. 4a. The first tangent is drawn based on the hydration plateau and the second tangent coincides with the maximum speed of water uptake.

The measured deliquescence point, reported in Fig. 4b, of pure K_2CO_3 corresponds well with the literature value (Greenspan, 1976). Further, the deliquescence points of the composites are lower than that of pure K_2CO_3, and larger amounts of CsF enhance the effect. This behaviour agrees with the mutual deliquescence point (MDRH) theory which states that in a mixture of deliquescent compounds, the deliquescence relative humidity (DRH) of the individual compounds will be lower than the DRH they exhibit in their pure form (Mauer and Taylor, 2010).

If we look at the results from DVS measurements as a whole, we see that the overall behaviour of composites is very similar to that of pure K_2CO_3, yet both hydration and deliquescence of composites are shifted to lower humidity. It may be caused by the distinct phase change of the additive, or it may be an indication of the modified phase change of K_2CO_3.

3.3. Impact on metastable zone

From the DVS measurements presented in Fig. 4, we notice that composite materials start taking up water at lower vapour pressures than pure K_2CO_3. We will now further investigate this phenomenon with the aid of TGA, and water desorption measurements will expand the investigation. Those measurements were conducted at a fixed vapour pressure of 12 mbar between 25 and 130 °C, and the gathered data are summarised in Fig. 5.

If we first consider hydration, we see that the water uptake starts at higher temperatures in salt mixtures than in pure K_2CO_3, and it is more prominent with increasing amounts of CsF. It correlates well with the isothermal DVS data in Fig. 4, which is a complementary effect at isobaric conditions. For the 10:1 and 20:1 composite, we observe

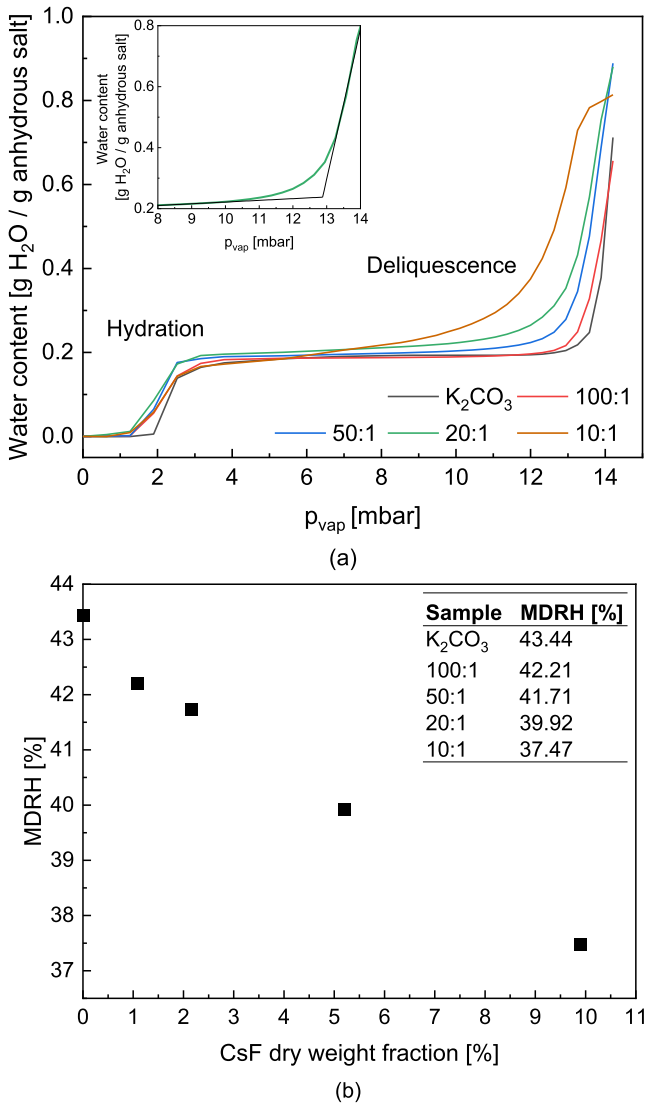

Fig. 4. a) Sorption curves measured at 25 °C between 0 and 45% RH. The insert gives an example of the determination of deliquescence point for 20:1 sample b) measured mutual deliquescence relative humidity (MDRH) as a function of CsF content in the sample with exact values given in the inserted table.

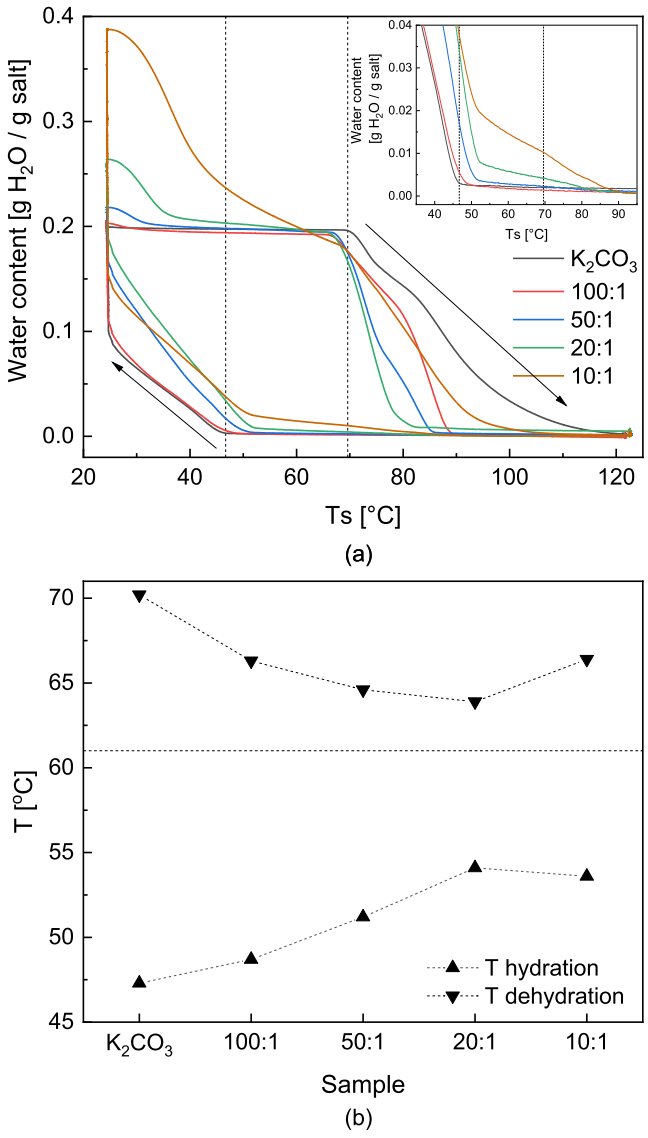

Fig. 5. a) Measured water content as a function of measured sample temperature for pure K_2CO_3 and K_2CO_3-CsF composites. The black arrows show the reaction direction, while the dashed lines mark the reaction onset temperatures of pure K_2CO_3 insert zooms in on the onset of hydration b) Measured reaction onset points for hydration ▲ and dehydration ▼at 12 mbar. The horizontal dashed line indicates an equilibrium temperature of 61 °C at 12 mbar. The heating tare is 1 °C/min.

pronounced 2-step hydration. The first mass increase occurs between 80 and 90 °C. However, due to the high hygroscopicity of CsF and the impact of deliquescence point lowering, we cannot distinguish between hydration and deliquescence of the additive. The second mass increase occurs at approximately 50 °C, coinciding with the hydration temperature of K_2CO_3. This 2-step process is not as evident in composites with lower amounts of CsF, most likely due to insensitivity of the measurement conditions.

Similarly to DVS measurements, salt mixtures' overall water uptake is larger. The 10:1 sample shows substantial water uptake, pointing to the deliquescence of the additive and K_2CO_3. Looking back to the MDRH points in the inset of Fig. 4b, we see that the humidity reaches 40 % RH during the TGA measurement, thus passing the 37.47 % MDRH point for the 10:1 composite.

If we now look at the dehydration, we can see several mass loss steps. We infer that the first mass loss, starting simultaneously with the temperature ramp, relates to the efflorescence of the additive. We base this assumption on the nearly simultaneous mass decrease and temperature increase. It shows that the absorbed water is very susceptible to slight environmental changes, meaning it is highly mobile and not bound to salt. Moreover, the measurement conditions are kept below the deliquescence of pure K_2CO_3 and below MDRH of most of the composites, as established in Fig. 4. As the temperature increases, the dehydration of K_2CO_3 starts in a regime comparable to pure salt. In all cases, adding CsF lowers the onset temperature of dehydration. It also enhances the reaction speed as a total conversion is achieved at lower temperatures than pure K_2CO_3, thus in a shorter time because identical heating rates are used for all experiments. The only exception is the 10:1 composite, where dehydration is the slowest of all composites. It is most likely caused by extensive MDRH lowering that leads to the deliquescence of K_2CO_3, which affects its dehydration behaviour.

From data gathered in Fig. 5a, we have established reaction onset temperatures that are summarised in Fig. 5b. In all cases, the addition of CsF shrinks MSZ of K_2CO_3 from 22.9 °C for pure K_2CO_3 to 9.8 °C for the 20:1 sample. Moreover, the temperature shift is more significant in the case of dehydration than hydration, which decreased up to 68.5 % and 49.6 %, respectively. Those findings show that the MSZ can be positively

affected by the presence of a deliquescent additive.

3.4. Cyclic stability

The reaction onset measurements have shown that all samples can be fully (de)hydrated at least once. Nevertheless, a viable TCM material must undergo numerous (de)hydration cycles. Because 10:1 composite is much more hygroscopic than any other samples, it undergoes deliquescence at conditions where other composites are stable. It means that handling the material becomes difficult, and reproducibility of the results cannot be guaranteed. For those reasons, we have excluded it from any further examination. The cyclic stability was investigated for the remaining samples over 10 cycles. Dehydration was conducted at 130 °C and 0 mbar, while hydration was done at isobaric-isothermal conditions of 30 °C and 12 mbar as described in point 2 of Section 2.2.4.

In Fig. 6, we summarised the results of those measurements. Analogously to previous TGA and DVS measurements, we see that with the increasing content of the additive in the composite, the amount of water absorbed by the sample increases. Moreover, the 20:1 sample exhibit fast and steady reaction kinetics from the first cycle, while the other samples have a significantly lower reaction rate on the first cycle compared to further cycles and the 20:1 composite as well, as shown in Fig. 6b. Furthermore, pure K_2CO_3 achieves complete hydration only on its sixth cycle at given conditions, while the remaining composites exhibit a stable hydration rate from the second cycle onwards.

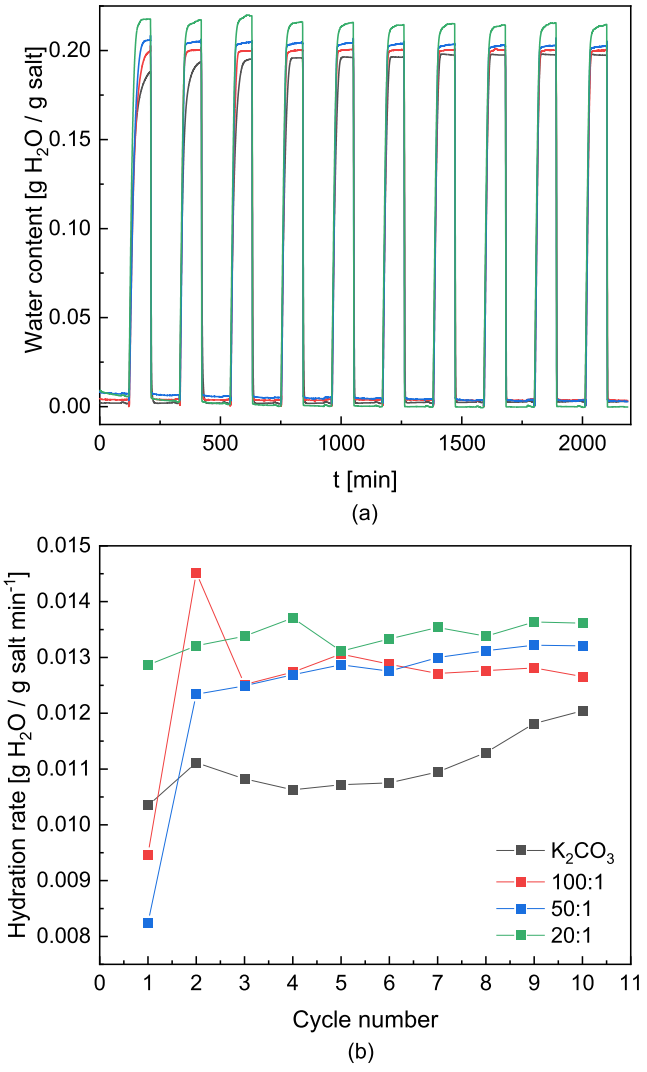

Fig. 6. Cyclic stability measurement with 10 (de)hydration cycles. Dehydration was conducted at 130 °C and 0 mbar, hydration was conducted at 30 °C 12 mbar a) Measured water content in a sample as a function of time b) Maximum hydration rate measured for subsequent cycles. Black – pure K_2CO_3, red – 100:1, blue – 50:1 and green – 20:1 sample. (For interpretation of the references to colour in this figure legend, the reader is referred to the web version of this article.)

Looking closer at the hydration speed, shown in Fig. 6b, we see that the reaction rate of pure K_2CO_3 starts to increase only after 5 cycles suggesting a necessary break-in period for the pure compound (Bevingt et al., 2020; Gaeini et al., 2019; Stanish and Perlmutter, 1984b), which is ascribed to defect and crack formation. On the other hand, the 20:1 sample presents an overall higher and more stable rate from the first cycle. This is thus more surprising than the low reaction kinetics of the first cycle, suggesting that the secondary phase may act as a defect-promoting agent. On average, the hydration rate is improved by 15–20 % with the addition of CsF.

3.5. Isobaric-isothermal reaction kinetics

Finally, with cyclic stability proved, we can investigate the reaction kinetics of the cycled samples at several isobaric and isothermal conditions. The measurements were conducted at 3 different temperatures, depicted in Fig. 1, and two different regions: outside the MSZ, where the driving force is large and the reaction is not obstructed by a nucleation barrier and within MSZ, where the reaction is inhibited. The exact measurement conditions are summarised in Table 2. This investigation aims to explore trends (de)hydration behaviour in a qualitative manner induced by varying CsF content.

First, we will look at hydration behaviour at 43.5 °C presented on the top of Fig. 7. When we investigate reaction kinetics outside the MSZ (Fig. 7a), we see that all samples behave similarly. In particular, pure K_2CO_3 and 100:1 samples show very similar rates, while the hydration rates of samples with higher CsF content are approximately 35 % higher. As we move into the MSZ (Fig. 7b), the 20:1 sample is the only one that achieves complete hydration within the allocated time. In addition to enhancing reaction kinetics and sorption properties, the addition of CsF significantly reduces the induction period within MSZ. For 20:1 and 50:1 samples, the induction period is non-existent, while for the 100:1 sample it is 50 % shorter than for pure K_2CO_3. This result agrees well with the narrowing of MSZ measured in Fig. 5. It is worth noticing that all composites exhibit instantaneous water uptake when humidity is applied. Since this phenomenon is present only in composites, we can assume that it is due to water sorption by the additive, as it is much more hygroscopic than K_2CO_3 and can undergo hydration if not even deliquescence at those conditions.

Now let us zoom in on dehydration kinetics, presented at the bottom of Fig. 7, which were investigated at similar supersaturations as the hydration kinetics. Outside the MSZ (Fig. 7c), pure K_2CO_3 and 100:1 samples present very poor kinetics and an induction period. On the contrary, the 20:1 and 50:1 samples have nearly twice as fast dehydration rate as pure K_2CO_3 and no induction period. The presence of the induction period might seem unexpected based on the MSZ boundaries presented in Fig. 1. However, it should be noted that the MSZ boundary was established with a scanning rate of 0.1 °C/min and extrapolated from data gathered at higher temperatures and vapour pressures (Sögütoglu et al., 2019). A slow scanning speed allows for a long nucleation period at the edge of MSZ, which is not present in this measurement. Moreover, an extrapolation of data collected at higher temperatures could lead to deviations at low temperatures, where dehydration is inherently inhibited. Moreover, this measurement requires a large jump in humidity from 19 mbar to 0.6 mbar, where we can expect a slight delay between the change in vapour pressure supplied by the external humidifier and the humidity experienced by the sample. Considering all those factors, the presence of a short induction period is within the margin of error for this measurement. The dehydration profiles of the remaining samples are comparable within the allocated time,

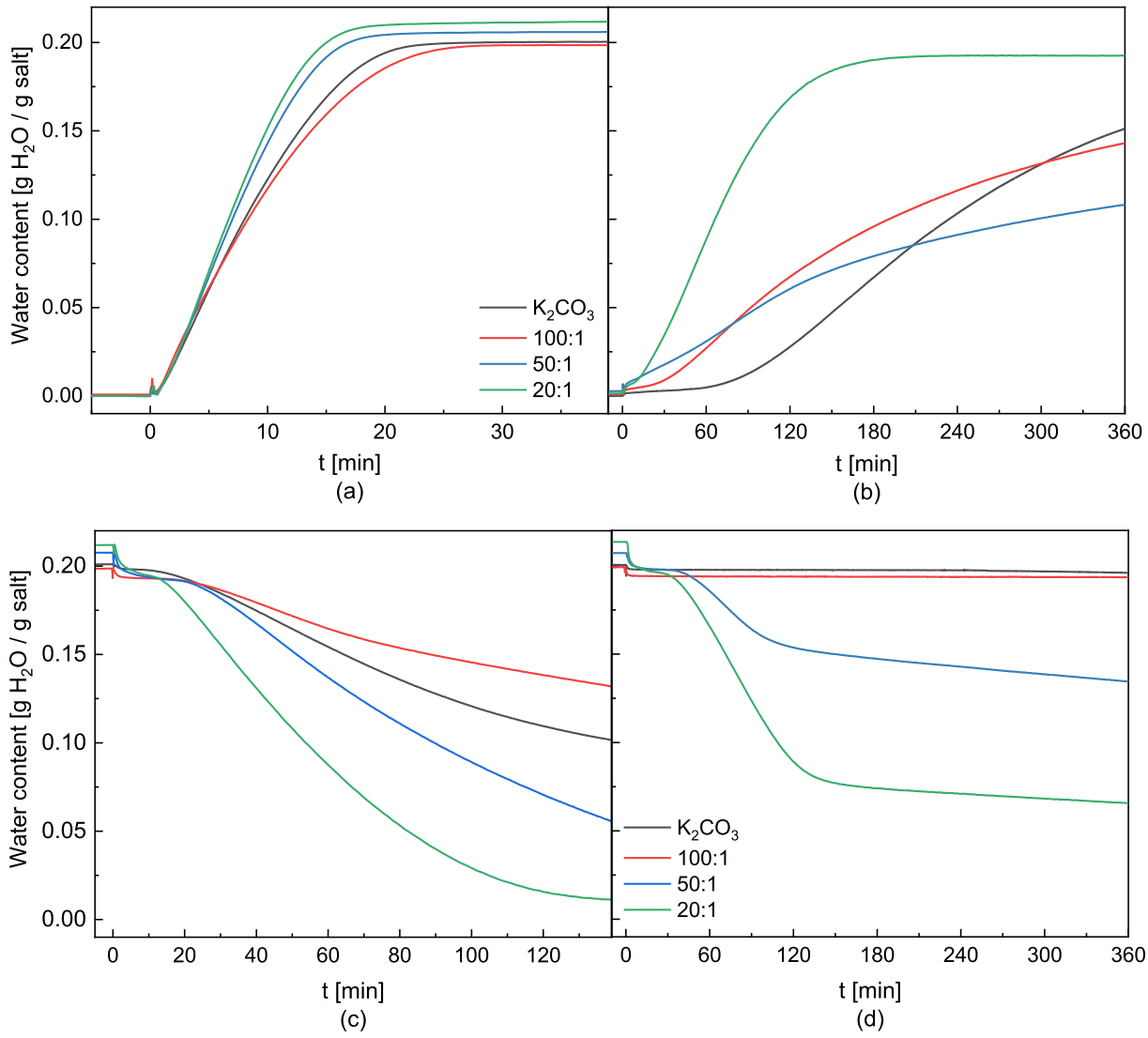

Fig. 7. Top: Hydration kinetics at 43.5 °C and a) 19 mbar and b) 6.7 mbar. Bottom: Dehydration kinetics at 43.5 °C and c) 0.6 mbar and d) 1.7 mbar. Black – pure K_2CO_3, red – 100:1, blue – 50:1 and green – 20:1 sample. (For interpretation of the references to colour in this figure legend, the reader is referred to the web version of this article.)

indicating an insufficient amount of the secondary phase to promote the dehydration of K_2CO_3. Lastly, if we look at the final loading of the 20:1 sample, we see that it begins to equilibrate at about 0.1 g H_2O / g salt, suggesting that not all water is driven out of the material under those conditions.

As the driving force for dehydration decreases and we move into the MSZ (Fig. 7d), a remarkable phenomenon develops for composites with a large amount of additive. After initial fast dehydration, the reaction rate slows down drastically. There is an indication of 2-step dehydration of pure K_2CO_3 already outside of MSZ, where at 40 % conversion (90 min into dehydration), the reaction rate slows down by 70 % compared to the initial reaction rate. This behaviour is only enhanced by the presence of the additive, where dehydration of 50:1 and 20:1 samples is nearly halted after the initial mass loss. Nevertheless, the induction period is drastically shortened in both samples as neither pure K_2CO_3 nor 100:1 sample has shown significant water loss during the 6 h, which again correlates with the previously established reaction onset points in Fig. 5.

To see how representative observed (de)hydration behaviour at 43.5 °C is, we have conducted similar measurements at 49 °C and 54 °C on pure K_2CO_3 and the two samples with the highest CsF content. Since the 100:1 sample has shown kinetic behaviour resembling pure K_2CO_3, it has been excluded from further evaluation. The data from those measurements can be seen in Appendix B.

During those measurements, we observed that the hydration kinetics at 49 °C and 54 °C are similar to at 43.5 °C. Outside of the MSZ, the impact of additive on the reaction kinetics is small, but the total water content in the sample is larger than in pure K_2CO_3. If the reaction kinetics are evaluated inside the MSZ, composites show faster kinetics by at least 57 %. Nonetheless, the overall water content decreases and becomes comparable with pure K_2CO_3.

The addition of CsF strongly enhances dehydration only far outside of MSZ. Furthermore, at elevated temperatures, the 2-step dehydration becomes more striking both for composites and pure K_2CO_3. Finally, the water retention by composites towards the end of dehydration becomes even more pronounced, indicating that a salt hydrate with high dehydration temperatures is present in the composite.

4. Discussion

Results presented in Section 3 indicate a complex interplay between several salts. In the first instance, the PXRD study in Fig. 2 shows that we are most likely looking at a mixture of at least three salts: K_2CO_3, KF, Cs_2CO_3, as discussed in 3.1.1, and potentially CsF as well as it is used

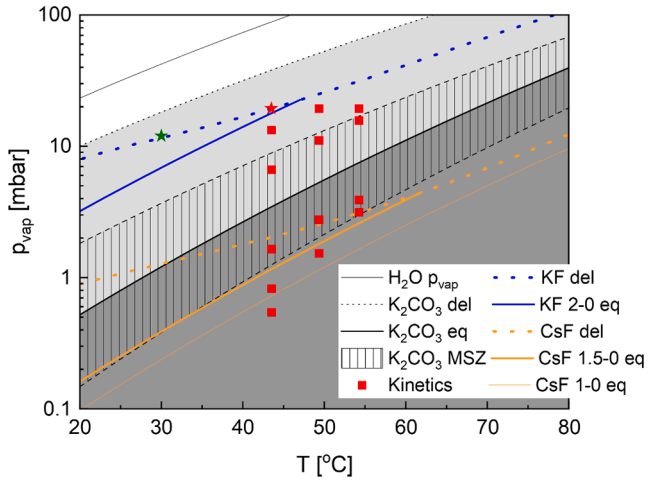

Fig. 8. Phase diagram of potassium carbonate (black lines) indicating measurement conditions of isobaric-isothermal kinetics (red points) and hydration during cycling (green point) together with known phase transitions of secondary phases (KF-blue, CsF-orange) present in the composite. Dotted lines show deliquescence (del) conditions based on (Greenspan, 1976), and solid lines show equilibrium lines (eq) based on (Aylward and Findlay, 2008; Glasser and Jenkins, 2007). (For interpretation of the references to colour in this figure legend, the reader is referred to the web version of this article.)

during the synthesis. It means that when we study phase transitions of K_2CO_3, we are also looking at phase transitions of all those salts. Both CsF and Cs_2CO_3 are considered highly hygroscopic salts, and they are known to form hydrates (Dobrynina and Dzyatkevich, 1967; Glasser, 2014; Reisman, n.d.). In Fig. 8, we have compiled reported thermodynamic data for three out of four potential salts present in the composite to get a better idea of the possible transitions at different measurement conditions.

By studying the phase diagram, we see that during most hydration measurements, we have solid $K_2CO_3{\cdot}1.5H_2O$ and $KF{\cdot}2H_2O$. It means that any added mobility in the form of a liquid-like layer must come from Cs-salt. The two conditions during which all secondary phases are deliquescent are cyclic stability measurement (30 °C and 12 mbar, green star in Fig. 8) and hydration measurement at 43.5 °C and 19 mbar (red star in Fig. 8). It is reflected in the water content in the sample, where the highest recorded loading is larger than what we would expect from salt hydration only. Further, the remaining hydration measurements resulted in different final water content, either due to the varying hydration state of the constituent salts or the mobile water content in the deliquescent salt solution.

The SEM-BSE images show that the Cs-rich secondary phase resides between grains and grain cracks due to capillary forces acting on it during high humidity conditions. This location, however, is valid only for a fully anhydrous state. When the material is exposed to high enough humidity, the Cs-salt will undergo deliquescence and form a liquid-like layer on top of K_2CO_3 grains. Therefore, it was postulated that MSZ exists due to a nucleation barrier (Sögütoglu et al., 2021). Thus, narrowing of MSZ must correspond to lowering of the nucleation barrier, which could be achieved in two ways. Firstly, the additional liquid in the system generated from the deliquescence of the additive could modify the supersaturation experienced by K_2CO_3, as illustrated in Fig. 9. Secondly, the additive could act as a nucleating agent or form imperfections in K_2CO_3 that act as nucleation centra.

The case of dehydration is more complicated, as the addition of CsF induced a new dehydration behaviour in K_2CO_3. The dehydration is enhanced mainly far outside of the MSZ. However, in many cases, the composite retained part of the absorbed water at the end of the dehydration. It could be due to lower hydrates of the secondary phases being stable under those conditions. As the dehydration conditions move closer to the equilibrium line, initially, we observe fast dehydration followed by a drastic drop in the reaction rate in 20:1 and 50:1 samples. From the measured shrinkage of MSZ, shown in Fig. 5, we can expect an enhanced reaction closer to the equilibrium since the narrowing of MSZ indicates a lowering of the nucleation barrier that hampers the phase change. It is supported by shorter induction periods observed during isobaric-isothermal measurements in MSZ. The lowering of the nucleation barrier could be caused by the additive acting as a defect or nucleation centre for the anhydrous phase (Heijmans, 2021). A subsequent sudden drop in the reaction rate is much more unexpected, and there are two possible causes. Firstly, it has been noticed that even pure K_2CO_3 exhibits tailing in dehydration, which could be a sign of a multistep nucleation and growth process (Deshpande et al., 1983). If multiple nucleation barriers need to be overcome, the presence of the secondary phases might affect them differently, leading to striking dehydration behaviour.

The second possibility is that highly hygroscopic salts retain water by

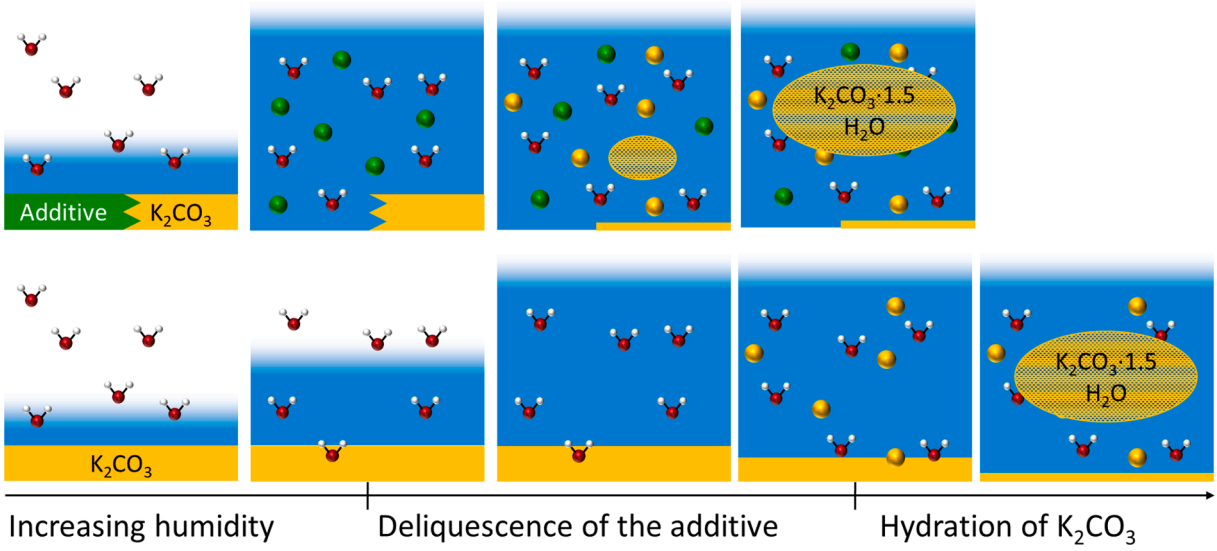

Fig. 9. Schematic representation of the processes occurring during K_2CO_3 (yellow) hydration with (top) an additive (navy) and without (bottom). The balls represent ions formed during local dissolution in a liquid-like layer (blue area) increasing with increasing humidity, represented by the black arrow. (For interpretation of the references to colour in this figure legend, the reader is referred to the web version of this article.)

remaining in the liquid-like layer. It would prevent complete dehydration of the composite, and only parts of the sample that are directly exposed to the gas flow or poor in additive could dehydrate quickly. The remainder of the sample would experience diffusion issues due to the liquid phase resulting in a slower dehydration rate.

By comparing all thermogravimetric measurements, we can notice a trade-off between the amount of CsF added, composite performance and its stability. High CsF content shrinks MSZ, meaning that lower vapour pressures are needed to achieve fast hydration. At the same time, the MDRH is lowered, which limits the maximum humidity material can withstand without losing its mechanical integrity. On top of that, the dehydration becomes inhibited at elevated vapour pressures despite being significantly enhanced outside MSZ. Finally, partial material deliquescence can lead to agglomeration, which is often undesired in practical applications as it lowers the material's permeability and obstructs water vapour transport (Fisher et al., 2021).In some cases, salt mixtures were engineered to prevent overhydration and agglomeration (Druske et al., 2014; Korhammer et al., 2016). In the composites investigated in this study, the 20:1 composition seems to be the most optimal. Higher CsF content lead to extensive MDRH lowering, while lower CsF contents have limited to no effect.

5. Conclusion

In this work, we investigated the impact of secondary phases incorporated through recrystallisation on the (de)hydration behaviour of K_2CO_3. Through PXRD, we found that CsF can react with K_2CO_3 during synthesis, forming KF. The SEM study has shown that secondary phases are not incorporated into the K_2CO_3 structure but reside between grains and in cracks of the primary phase. Analysis of sorption properties shows that K_2CO_3-CsF composites can absorb larger amounts of water than pure K_2CO_3. The excess water in the composite is due to the deliquescence of the added salt as it exceeds amounts that could be accounted for by hydration. We have determined that the width of MSZ can be shrunk by 5–13 °C with the addition of CsF, but it also induces MDRH lowering of up to 6 % or 1.9 mbar.

Cyclic stability measurements have shown that the salt mixtures are stable over at least 10 (de)hydration cycles. Isobaric and isothermal reaction kinetics at several temperatures have shown that composites with sufficiently high additive content (20 mol K_2CO_3: 1 mol additive) possess enhanced hydration kinetics at all investigated points. In the case of dehydration, the additive can have both positive and negative effects. Within MSZ, it eliminates the induction period, but the reaction proceeds in an unusual 2-step fashion, with the second step slower than dehydration of pure K_2CO_3. Most likely, diffusion limitations cause the sudden drop in dehydration speed within MSZ, which is not an issue outside MSZ, where the secondary phase enhances the dehydration reaction.

Based on the observations, we believe that the hydration reaction is enhanced by the added wetting layer formed by the deliquescent secondary salt. Defects can enhance the dehydration within the structure formed during the recrystallisation of the salt mixture, but the diffusion can also limit it through the added wetting layer. A more detailed study on salt interaction in a multi-component system is needed to fully understand the complex phase transition behaviour. With a better understanding of how the individual compounds affect each other's phase transitions and stability in the presence of water vapour, an optimal composition and operating conditions could be designed.

Declaration of Competing Interest

The authors declare that they have no known competing financial interests or personal relationships that could have appeared to influence the work reported in this paper.

Acknowledgement

This publication is part of the project Mat4Heat with project number 739.017.014 of the research programme Mat4Sus which is financed by the Dutch Research Council (NWO).

The authors would like to thank Jelle Rohlfs and Hans Dalderop for their technical support.

References

Afflerbach, S., Trettin, R., 2019. A systematic screening approach for new materials for thermochemical energy storage and conversion based on the Strunz mineral classification system. Thermochim Acta 674, 82–94. https://doi.org/10.1016/j.tca.2019.02.010.

Aylward, G., Findlay, T., 2008. SI Chemical Data Book, 6th ed. John Wiley & Sons Australia.

Beving, M.A.J.M., Frijns, A.J.H., Rindt, C.C.M., Smeulders, D.M.J., 2020. Effect of cycle-induced crack formation on the hydration behaviour of K2CO3 particles: Experiments and modelling. Thermochim Acta 692, 178752. https://doi.org/10.1016/j.tca.2020.178752.

Clark, R.-J., Gholamibozanjani, G., Woods, J., Kaur, S., Odukomaiya, A., Al-Hallaj, S., Farid, M., 2022. Experimental screening of salt hydrates for thermochemical energy storage for building heating application. J. Energy Storage 51, 104415.

Deshpande, D.A., Ghormare, K.R., Deshpande, N.D., Tankhiwale, A. V, 1983. DEHYDRATION OF CRYSTALLINE K2C03-1.5 H2O 66, 255–265.

Dobrynina, T.A., Dzyatkevich, B.S., 1967. Investigation of peroxyhydrates and hydrates of rubidium and cesium carbonates: Communication 5. Physicochemical investigation of the binary systems Rb2CO3-H2O and Cs2CO3-H2O. Russ. Chem. Bull. 16 (4), 703–706.

Donkers, P.A.J., Sögütoglu, L.C., Huinink, H.P., Fischer, H.R., Adan, O.C.G., 2017. A review of salt hydrates for seasonal heat storage in domestic applications. Appl. Energy 199, 45–68. https://doi.org/10.1016/j.apenergy.2017.04.080.

Druske, M.M., Fopah-Lele, A., Korhammer, K., Rammelberg, H.U., Wegscheider, N., Ruck, W., Schmidt, T., 2014. Developed materials for thermal energy storage: Synthesis and characterisation. Energy Procedia 61, 96–99. https://doi.org/10.1016/j.egypro.2014.11.915.

Fisher, R., Ding, Y., Sciacovelli, A., 2021. Hydration kinetics of K2CO3, MgCl2 and vermiculite-based composites in view of low-temperature thermochemical energy storage. J. Energy Storage 38, 102561.

Gaeini, M., Shaik, S.A., Rindt, C.C.M., 2019. Characterisation of potassium carbonate salt hydrate for thermochemical energy storage in buildings. Energy Build. 196, 178–193. https://doi.org/10.1016/j.enbuild.2019.05.029.

Glasser, L., 2014. Thermodynamics of inorganic hydration and of humidity control, with an extensive database of salt hydrate pairs. J. Chem. Eng. Data 59 (2), 526–530. https://doi.org/10.1021/je401077x.

Glasser, L., Jenkins, H.D.B., 2007. The thermodynamic solvate difference rule: Solvation parameters and their use in interpretation of the role of bound solvent in condensed-phase solvates. Inorg. Chem. 46, 9768–9778. https://doi.org/10.1021/ic701105p.

Greenspan, L., 1977. Humidity fixed points of binary saturated aqueous solutions. J. Res. Natl. Bur Stand. - A. Phys ics Chem. 81A (1), 89. https://doi.org/10.6028/jres.081A.011.

Heijmans, K., 2021. Thermochemical energy storage : advances in molecular modeling.

Idemoto, Y., Richardson, J.W., Koura, N., Kohara, S., Loong, C.-K., 1998. Crystal structure of (LixK1 − x)2CO3 (x = 0, 0.43, 0.5, 0.62, 1) by neutron powder diffraction analysis. J. Phys. Chem. Solids 59 (3), 363–376. https://doi.org/10.1016/S0022-3697(97)00209-6.

Korhammer, K., Druske, M.M., Fopah-Lele, A., Rammelberg, H.U., Wegscheider, N., Opel, O., Osterland, T., Ruck, W., 2016. Sorption and thermal characterisation of composite materials based on chlorides for thermal energy storage. Appl. Energy 162, 1462–1472. https://doi.org/10.1016/j.apenergy.2015.08.037.

Li, W., Zeng, M., Wang, Q., 2020. Development and performance investigation of MgSO4/SrCl2 composite salt hydrate for mid-low temperature thermochemical heat storage. Sol. Energy Mater. Sol. Cells 210, 110509. https://doi.org/10.1016/j.solmat.2020.110509.

Linnow, K., Niermann, M., Bonatz, D., Posern, K., Steiger, M., 2014. Experimental studies of the mechanism and kinetics of hydration reactions. Energy Procedia 48, 394–404. https://doi.org/10.1016/j.egypro.2014.02.046.

Mauer, L.J., Taylor, L.S., 2010. Water-Solids Interactions: Deliquescence. Annu. Rev. Food Sci. Technol. 1 (1), 41–63. https://doi.org/10.1146/annurev.food.080708.100915.

N'Tsoukpoe, K.E., Schmidt, T., Rammelberg, H.U., Watts, B.A., Ruck, W.K.L., 2014. A systematic multistep screening of numerous salt hydrates for low temperature thermochemical energy storage. Appl. Energy 124, 1–16. https://doi.org/10.1016/j.apenergy.2014.02.053.

Posern, K., Kaps, C.h., 2010. Calorimetric studies of thermochemical heat storage materials based on mixtures of MgSO4 and MgCl2. Thermochim Acta 502 (1-2), 73–76. https://doi.org/10.1016/j.tca.2010.02.009.

Rammelberg, H.U., Myrau, M., Schmidt, T., Ruck, W.K., 2013. An optimisation of salt hydrates for thermochemical heat storage. Touka Shobo Innov. Mater. Process. Energy Syst. Bidyut Baran Saha, Michihisa Koyama, Yasuyuki Tak. Yoshinori Hamamoto, Tak. Miyazaki, Kohno Masamichi, Kohei Ito. IMPRES 550–555.

Rammelberg, H.U., Osterland, T., Priehs, B., Opel, O., Ruck, W.K.L., 2016. Thermochemical heat storage materials – Performance of mixed salt hydrates. Sol. Energy 136, 571–589. https://doi.org/10.1016/j.solener.2016.07.016.

Rehman, A.U., Khan, M., Maosheng, Z., 2019. Hydration behavior of MgSO 4 -ZnSO 4 composites for long-term thermochemical heat storage application Hydration behavior of MgSO 4 – ZnSO 4 composites for long-term thermochemical heat storage application. J. Energy Storage 26, 101026. https://doi.org/10.1016/j.est.2019.101026.

Reisman, A., n.d. Isobaric Dissociation Studies of Alkali Metal Carbonate Hydrates Using Simultaneous Differential Thermal Analysis-Thermogravimetric Analysis.

Richter, M., Habermann, E.M., Siebecke, E., Linder, M., 2018. A systematic screening of salt hydrates as materials for a thermochemical heat transformer. Thermochim Acta 659, 136–150. https://doi.org/10.1016/j.tca.2017.06.011.

Skakle, J.M.S., Wilson, M., Feldmann, J., 2001. Dipotassium carbonate sesquihydrate: rerefinement against new intensity data. Acta Crystallogr. Sect. E Struct. Reports Online 57, i94–i97. https://doi.org/10.1107/S1600536801016312/BT6075ISUP2.HKL.

Sögütoglu, L.-C., Steiger, M., Houben, J., Biemans, D., Fischer, H.R., Donkers, P., Huinink, H., Adan, O.C.G., 2019. Understanding the Hydration Process of Salts: The Impact of a Nucleation Barrier. Cryst. Growth Des. 19 (4), 2279–2288. https://doi.org/10.1021/acs.cgd.8b0190810.1021/acs.cgd.8b01908.s001.

Sögütoglu, L.-C., Birkelbach, F., Werner, A., Fischer, H., Huinink, H., Adan, O., 2021. Hydration of salts as a two-step process: Water adsorption and hydrate formation. Thermochim Acta 695, 178819. https://doi.org/10.1016/j.tca.2020.178819.

Sögütoglu, L.C., Donkers, P.A.J., Fischer, H.R., Huinink, H.P., Adan, O.C.G., 2018. In-depth investigation of thermochemical performance in a heat battery: Cyclic analysis of K2CO3, MgCl2and Na2S. Appl. Energy 215, 159–173. https://doi.org/10.1016/j.apenergy.2018.01.083.

Stanish, M.A., Perlmutter, D.D., 1984a. Rate processes in cycling a reversible gas-solid reaction. AIChE J. 30 (1), 56–62. https://doi.org/10.1002/aic.690300110.

Stanish, M.A., Perlmutter, D.D., 1984b. Kinetics of hydration-dehydration reactions considered as solid transformations. AIChE J. 30 (4), 557–563. https://doi.org/10.1002/aic.690300405.

Vaitkus, A., Merkys, A., Gražulis, S., 2021. Validation of the Crystallography Open Database using the Crystallographic Information Framework. J. Appl. Crystallogr. 54 (2), 661–672.

Wyckoff, R.W.G., 1963. Interscience publishers, new york, new york rocksalt structure. Cryst. Struct. 1, 85–237.

Zhao, Q., Lin, J., Huang, H., Xie, Z., Xiao, Y., 2022. Enhancement of heat and mass transfer of potassium carbonate-based thermochemical materials for thermal energy storage. J. Energy Storage 50, 104259.